International Journal of Women's Health

Dovepress
Taylor & Francis Group

Open Access Full Text Article

ORIGINAL RESEARCH

Identification of Bacterial Lipopolysaccharide-Related Molecular Subtypes and Development of a Four-Gene Prognostic Risk Model in Cervical Cancer

Yuehong Tong[1], Lili Xu[1], YiQun Sun[2], Keke Zhang[1], Xiaoyan Fu[3]

[1]Department of Gynaecology, Affilitated Jinhua Hospital, Zhejiang University School of Medicine, Jinhua, Zhejiang, 321000, People's Republic of China; [2]Department of Gynaecology, Jinhua Maternal and Child Health Care Hospital, Jinhua, Zhejiang, 321000, People's Republic of China; [3]Medical Molecular Biology Laboratory, Medical College, Jinhua University of Vocational Technology, Jinhua, Zhejiang, 321000, People's Republic of China

Correspondence: Xiaoyan Fu, Medical Molecular Biology Laboratory, Medical College, Jinhua University of Vocational Technology, No. 1188, Wuzhou Street, Wucheng District, Jinhua, Zhejiang, 321000, People's Republic of China, Tel +86-13586976775, Email XiaoyanFu1010@163.com

International Journal of Women's Health downloaded from https://www.dovepress.com/
For personal use only.

Background: Cervical cancer (CC) ranks among the top causes of cancer-related illness and death in women worldwide. Bacterial lipopolysaccharide-related genes (LRGs) contribute to tumor progression and immunosuppression. This study aimed to identify CC molecular subtypes based on LRGs and construct a prognostic model to explore patient prognosis and immune features.

Methods: Transcriptomic data and corresponding clinical details for CC patients were obtained from publicly accessible resources such as The Cancer Genome Atlas (TCGA) and the Genotype-Tissue Expression (GTEx) project. Molecular subtypes were uncovered by applying non-negative matrix factorization (NMF) to prognostic LRGs. Significant prognostic genes were identified through Cox regression coupled with Shrinkage and Selection Operator (LASSO) analysis to build a risk model, which was then validated using an independent dataset from the Gene Expression Omnibus (GEO). RT-qPCR validated gene expression. Differences in prognosis, tumor microenvironment (TME), immune status, and tumor mutational burden (TMB) were analyzed between risk groups, and drug sensitivity predictions were performed using pRRophetic.

Results: The study successfully identified two molecular subtypes. A prognostic model was developed based on four selected genes, with Receiver Operating Characteristic (ROC) curve analysis confirming its robust predictive performance in both the training and independent validation datasets. RT-qPCR analysis provided additional verification of the gene expression profiles. The low-risk cohort displayed a significantly more favorable outcome, along with increased infiltration of immune cells and enhanced immune scores. Furthermore, the signature genes were associated with sensitivity to multiple anticancer drugs, indicating potential therapeutic targets.

Conclusion: The risk model based on LRGs effectively predicts survival outcomes and immune characteristics in CC patients, providing a novel theoretical foundation for personalized treatment and immunotherapy strategies.

Plain Language Summary:

(1) In this study, four characteristic genes that can be used as prognostic biomarkers for cervical cancer were identified, namely *CXCL1*, *HLA-DRA*, *POSTN* and *TGFBI*.
(2) The study identified two cervical cancer molecular subtypes associated with bacterial lipopolysaccharide and established a prognostic risk model with strong predictive power.
(3) Patients classified as low-risk demonstrate better survival outcomes, increased immune cell infiltration, and greater responsiveness to immunotherapy than those in the high-risk group.

Keywords: cervical cancer, bacterial lipopolysaccharide-related genes, molecular subtypes, prognostic models, immunoassays

Received: 10 June 2025
Accepted: 5 September 2025
Published: 13 September 2025

© 2025 Tong et al. This work is published and licensed by Dove Medical Press Limited. The full terms of this license are available at https://www.dovepress.com/terms.php and incorporate the Creative Commons Attribution – Non Commercial (unported, v4.0) License (http://creativecommons.org/licenses/by-nc/4.0/). By accessing the work you hereby accept the Terms. Non-commercial uses of the work are permitted without any further permission from Dove Medical Press Limited, provided the work is properly attributed. For permission for commercial use of this work, please see paragraphs 4.2 and 5 of our Terms (https://www.dovepress.com/terms.php).

Introduction

Worldwide, cervical cancer (CC) is a prevalent and deadly tumor in women, significantly endangering female health.[1] As reported by the International Agency for Research on Cancer (IARC), CC is the fourth leading malignancy affecting women and is especially common in the 15–44 age group.[2] According to the World Health Organization, in 2020, there were approximately 604,000 new cases of CC and 342,000 related deaths documented worldwide, with over 85% of these occurring in developing nations where healthcare resources are limited.[3] This significant geographic variation is largely closely related to human papillomavirus (HPV) vaccination rates and the prevalence of CC screening. Despite the significant impact of CC screening and human papillomavirus (HPV) vaccination in prevention and early diagnosis, outcomes for patients with advanced CC remain poor, with five-year survival rates remains low.[4,5] In addition, the heterogeneity of tumours and the complex tumour microenvironment (TME) significantly affect the therapeutic efficacy of CC, making precision therapy a critical issue to be addressed.[6–9] Therefore, a detailed understanding of CC's molecular basis and identification of molecular subtypes and prognostic markers of clinical significance are important for achieving individualised precision treatment and improving patient prognosis.

The TME is crucial in the initiation, development, spread, and treatment outcomes of tumors.[10–12] The TME represents a complex and diverse system made up of tumor cells, immune cells, fibroblasts, vascular endothelial cells, and the extracellular matrix.[13] Among them, immune cell infiltration and inflammatory response are important factors affecting tumour progression and therapeutic efficacy.[14–17] It is well known that high-risk HPV infection is a major causative factor in the development of CC.[18,19] HPV disrupts the tumour suppressor mechanism of host cells through its oncogenic proteins, E6 and E7, and promotes aberrant cell proliferation and genomic instability.[20–22] In addition, HPV infection has been found to modulate the host immune response, suppressing antiviral and anti-tumour immunity, thus helping tumour cells evade immune surveillance.[23,24] Recently, bacterial lipopolysaccharide (LPS), a key structural molecule in Gram-negative bacteria, has been found to have a strong connection with the TME.[25–27] For example, LPS affects the immune status of the TME by activating pattern recognition receptors such as Toll-like receptor 4 (TLR4), which induces the release of inflammatory factors and immune cell activation.[28,29] It has been shown that the TLR4/NF-κB pathway is up-regulated in CC and is closely associated with tumour cell proliferation, migration and invasion.[30,31] Additionally, bacterial lipopolysaccharide-related genes (LRGs) have been shown to contribute significantly to tumor immune escape, influencing therapeutic efficacy and patient survival in multiple tumor forms.[32–34] However, the expression patterns, specific roles and potential mechanisms of LRGs in CC have not been systematically elucidated. Considering that HPV infection may affect the LPS level by altering the local flora composition of the cervix, which in turn affects the local immune microenvironment of the cervix, examining the role of LRGs in regulating immunity within CC could provide essential theoretical support for advancing immunotherapy development.[35,36]

This research utilized CC transcriptomic data combined from The Cancer Genome Atlas (TCGA) and the Genotype-Tissue Expression (GTEx) databases, combined with LRGs collected from Comparative Toxicogenomics Database (CTD), we systematically screened differentially expressed lipopolysaccharide-related genes (DELRGs), identified molecular subtypes of CC using non-negative matrix factorisation (NMF) method, and constructed a prognostic risk model. The connection between LRGs and the immune landscape of CC and therapeutic response was deeply explored through immune infiltration analysis, tumour mutation load (TMB) analysis and drug sensitivity prediction. This research offers a novel approach to molecular classification and prognosis evaluation of CC, while also building a foundation for personalized immunotherapy development.

Methods

Data Collection

The TCGA database (https://portal.gdc.cancer.gov) was utilized to obtain transcriptomic datasets for cervical cancer (CESC), which included mRNA expression profiles from 306 tumor and 3 normal samples, as well as copy number variation and clinical information. To ensure the reliability of the survival analyses, samples lacking follow-up survival information (eg, overall survival time as well as survival status) or missing key clinical variables (eg, stage, etc.) were excluded from subsequent analyses. In addition, 10 healthy cervical transcriptomes from the GTEx database (https://

xenabrowser.net/datapages/) were merged to form a training set. We verified our results using the GSE52903 microarray dataset available in the GEO database (https://www.ncbi.nlm.nih.gov/geo/). The keyword "lipopolysaccharide" was used to retrieve 6571 LRGs from the CTD (http://ctdbase.org/).

Analysis of LRGs

Batch effect correction of the combined TCGA and GTEx data using the ComBat algorithm. The "edgeR" package was employed to perform differential expression analysis, applying criteria of False Discovery Rate (FDR) below 0.05 and an absolute log fold change (FC) greater than 2. Following this, an intersection between differentially expressed genes (DEGs) and LRGs was performed to pinpoint DELRGs. Functional enrichment of these DELRGs was then assessed using the "clusterProfiler" tool. To identify DELRGs with prognostic significance, we excluded patients with survival times <30 days and performed univariate Cox regression analyses ($p < 0.01$). Additionally, the expression levels of gene in both normal and tumor tissues were quantified, and their correlations were evaluated.

Molecular Typing Based on DELRGs

NMF clustering was applied to the expression data of prognostically significant DELRGs, with two clusters (k=2) determined as the optimal grouping based on higher silhouette coefficient as well as higher dispersion. To evaluate the accuracy of subtype classification and its influence on survival outcomes, principal component analysis (PCA) and survival analysis were performed. Also, differential analysis of subtypes was performed to identify DEGs between subtypes. The functional roles of these genes were examined through pathway enrichment analysis based on the Kyoto Encyclopedia of Genes and Genomes (KEGG). Additionally, variations in immune cell infiltration among the subtypes were evaluated using ssGSEA, ESTIMATE, and MCP-counter algorithms, alongside a comparison of clinical characteristics.

Construction of Prognostic Risk Model

Clinical data and expression data from DEGs were combined and samples with survival < 30 days were excluded. Univariate Cox regression identified 23 candidate genes ($p < 0.01$). To minimize the impact of collinearity, prognostic genes were further refined using the Least Absolute Shrinkage and Selection Operator (LASSO) regression via the "glmnet" package. Subsequently, a multivariate Cox regression analysis was performed to establish a prognostic risk model comprising four genes. Based on their calculated risk scores, patients were stratified into high-risk and low-risk groups. The model's predictive performance was assessed using receiver operating characteristic (ROC) curves at 1, 3, and 5 years (AUC), alongside Kaplan-Meier (K-M) survival analysis. Additionally, the model's validity was confirmed using an independent dataset GSE52903.

Enrichment Analysis

To explore the pathway differences between the high-risk and low-risk groups, Gene Set Enrichment Analysis (GSEA, v4.3.2) was conducted. Concurrently, differential analysis was performed, and the resulting DEGs were analyzed for functional enrichment using the "clusterProfiler" package, which included Gene Ontology (GO) and KEGG pathway analyses.

Nomogram Based on Clinical Information and Risk Score

Univariate and multivariate Cox regression analyses were performed by integrating clinical variables with prognostic model risk scores. A nomogram was constructed to estimate patient survival probabilities at 1, 3, and 5 years. Decision Curve Analysis (DCA) was used to evaluate the clinical utility of the model, while calibration plots were generated to compare predicted outcomes against actual patient prognoses.

Subgroup Analysis Based on Risk Model of Clinicopathological Characteristics

Clinical features of TCGA-CESC patients were analyzed statistically alongside their prognostic risk scores. Patients were further stratified based on age, grade, stage, and TNM stage, with K-M survival curves were generated to compare high- and low-risk groups within each subgroup.

Immune Infiltration Analysis and Prediction of Immunotherapy Response

Scores reflecting the infiltration of 29 immune cell subsets and functions were generated using the ssGSEA method. Immune cell abundance in different risk groups was further evaluated with CIBERSORT, which also measured the expression of immune checkpoint molecules within these groups. Furthermore, the association between the genes defining the model signature and immune cell infiltration levels was examined using Pearson correlation analysis. To investigate potential differences in immunotherapy responses between patients classified as high-risk and low-risk, Immunophenoscore (IPS) data for TCGA-CESC cases were retrieved from The Cancer Immunome Atlas (TCIA, https://tcia.at), followed by comparative analysis of these groups. Immunotherapy strategies that inhibit immune checkpoints such as PD-1 or PD-L1 have garnered significant attention in recent research.[37,38] To evaluate how well risk scores predict responses to immunotherapy, we utilized clinical data from patients who received anti-PD-L1 therapy in the IMvigor210 cohort, accessed via the "IMvigor210CoreBiologies" R package. The developed model facilitated the categorization of samples into high- and low-risk categories, providing a basis to forecast their potential response to immunotherapy.

TMB Analysis and Drug Sensitivity Analysis

Mutation data from the TCGA-CESC cohort were used to calculate TMB scores for each sample, followed by Wilcoxon tests to compare TMB values between different risk groups. Additionally, the mutation profiles of the top 20 most frequently altered genes were summarized separately for each risk group to elucidate potential differences in mutational landscapes. To identify novel therapeutic targets and more effective treatments, the half maximal inhibitory concentration (IC50) of various agents was estimated using the "pRRophetic" package to predict drug sensitivity. The pRRophetic algorithm was based on the publicly available drug sensitivity database Genomics of Drug Sensitivity in Cancer (GDSC), which contained gene expression profiles of a wide range of tumour cell lines and experimentally measured IC50 values for a wide range of chemotherapeutic agents. Notably, a lower IC50 indicates greater drug efficacy against tumors. The CellMiner database (https://discover.nci.nih.gov/cellminer/) was utilized to identify drugs whose sensitivities were significantly correlated with the signature genes.

Construction of Regulatory Networks for Characteristic Genes

We utilized miRNet (https://www.mirnet.ca/) and NetworkAnalyst (https://www.networkanalyst.ca/) to identify miRNAs and transcription factors (TFs) associated with characteristic genes. The resulting networks were then visualized using Cytoscape v3.10.2.

Validation of Target Genes Using Quantitative Reverse Transcription PCR (RT-qPCR)

The human CC cell line SiHa was obtained from the American Type Culture Collection (ATCC, Manassas, VA, USA). Total RNA was extracted from these cells using TRIzol reagent (Invitrogen, USA). Subsequently, complementary DNA (cDNA) was synthesized from the isolated RNA employing the 5× ALL-IN-One RT Master Mix kit (Applied Biological Materials Inc., Canada). RT-qPCR assays were then performed on the ABI 7500 Fast Real-Time PCR System (Applied Biosystems, USA) using the TB Green Premix Ex Taq kit (Takara, Dalian, China). *GAPDH* served as the internal reference gene to normalize expression levels. Relative quantification of gene expression was calculated by applying the $2^{-\Delta\Delta Ct}$ method.[39] Detailed primer sequences used for amplification are listed in Table 1.

Statistical Analysis

R software (version 4.4.1) and its relevant packages were employed to conduct the analyses. Differences between the two groups were evaluated using Wilcoxon rank-sum tests and Student's t-tests. Survival outcomes were compared by generating K-M curves, with statistical significance determined through the Log rank test. The "timeROC" package was utilized to construct ROC curves, while data visualization was primarily carried out with the help of the "ggplot2" package. The relationship between the two variables was examined using both Spearman's rank correlation and Pearson's correlation analyses. The median was used to define the cutoff for subgroup analysis. A threshold of $p < 0.05$ was

Table 1 Detailed Primer Sequences Used in RT-qPCR

Gene	Primer Nucleotide Sequences (5'-3')
CXCL1	Forward: CTGGGATTCACCTCAAGAACATC
	Reverse: CAGGGTCAAGGCAAGCCTC
HLA-DRA	Forward: GGCGGCTTGAAGAATTTGGAC
	Reverse: CACAGGGCTGTTTGTGAGCA
POSTN	Forward: GCGAGATCATCAAGCCAGCAGAG
	Reverse: TCCAGTCTCCAGGTTGTGTCAGG
TGFBI	Forward: ATGACCCTCACCTCTATGTACC
	Reverse: CACAGTTCACAGTTACAATCCCA
GAPDH	Forward: CTGGGCTACACTGAGCACC
	Reverse: AAGTGGTCGTTGAGGGCAATG

considered statistically significant. The p-values were classified into groups as: ****p less than 0.0001; ***between 0.0001 and 0.001; **between 0.001 and 0.01; *ranging from 0.01 to 0.05; and ns indicating p-values greater than 0.05.

Results

Differential Expression Analysis of LRGs in CC

A total of 1,265 differentially expressed genes (DEGs) were identified, comprising 646 upregulated and 619 downregulated genes (Figure 1A). Intersection of these DEGs with LRGs resulted in 479 overlapping DELRGs (Figure 1B). Subsequent enrichment analyses, including GO (Figure 1C) and KEGG pathway analysis (Figure 1D), were conducted on this subset. GO molecular function enrichment revealed that these genes predominantly participate in mediating intercellular adhesion and chemokine activity, highlighting their roles in cell-to-cell and cell-to-extracellular matrix interactions. GO biological process analysis reveals that these genes play crucial roles in tissue development, preserving structural stability, and guiding cell differentiation. Cellular component analysis highlights the association of genes with the extracellular matrix and cellular junctions associated with maintaining the structural integrity of tissues, such as collagen-containing extracellular matrix and adherens junction. Enrichment analysis of KEGG pathways illuminated their

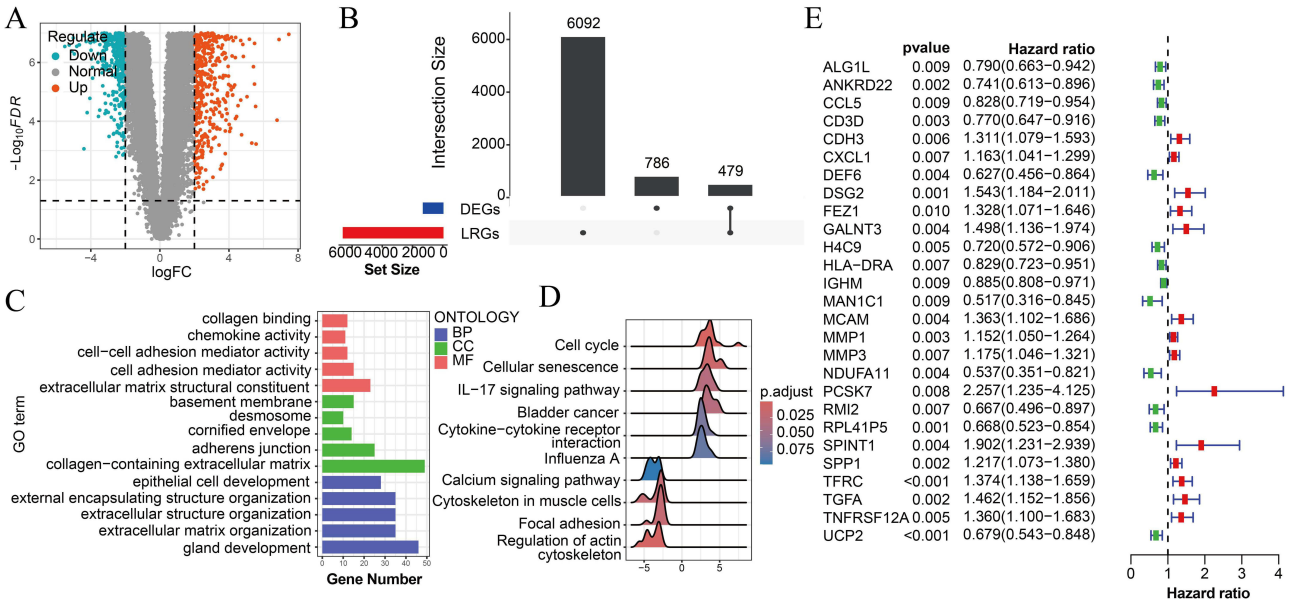

Figure 1 Analysis of DEGs in CC and normal groups and functional enrichment of LRGs. (**A**) Volcano plot of DEGs. (**B**) Intersection analysis of DEGs and LRGs (479 DELRGs). (**C**) GO enrichment analysis of intersected genes. (**D**) KEGG enrichment analysis of the intersected genes. (**E**) Univariate forest plot of prognostic genes ($p < 0.01$, 27 genes).
Abbreviations: CC, cellular composition; BP, biological process; MF, molecular function.

https://doi.org/10.2147/IJWH.S537092

critical roles in dynamic cellular processes, including cell division, senescence, signaling cascades, motility, and cytoskeleton control, eg Cell cycle and Cytoskeleton in muscle cells. A univariate Cox regression analysis was performed on the DELRGs using a significance cutoff of $p < 0.01$, which led to the identification of 27 genes associated with prognosis (Figure 1E, Supplementary Table S1). The expression analysis revealed that most of these genes were upregulated in tumor tissues compared to normal counterparts (see Supplementary Figure S1A). In addition, correlation analysis among these genes showed that most of them had a tight co-expression relationship, suggesting a possible synergistic role in tumour development (Supplementary Figure S1B).

Subtype Identification and Related Analysis

Using the expression profiles of the 27 prognostic genes identified through univariate Cox analysis, NMF was applied for clustering, resulting in two distinct groups (Figure 2A and B). Subsequently, PCA plots were drawn to visualise the clustering effect (Figure 2C). The survival analysis demonstrated that individuals in group 1 experienced notably worse outcomes than those in group 2 (Figure 2D), suggesting that the two subtypes had different prognostic characteristics. Figure 2E demonstrates the differential expression of these 27 prognostic genes in the two subgroups, with approximately half of them highly expressed in group1 and the other half in group2. Immune infiltration disparities between the subtypes, calculated via ssGSEA, are visualized in the heatmap of Figure 2F, highlighting variations in immune cell abundance. Using the ESTIMATE algorithm, the ESTIMATE, Immune, Stromal Scores, and Tumor Purity were assessed, revealing that group 1 had a notably lower immune score and higher tumor purity than group 2, suggesting enhanced immune infiltration and lower purity in group 2 (Figure 2G). MCP-counter analysis further confirmed that immune cell infiltration levels were significantly elevated in group 2 relative to group 1 (Figure 2H). Finally, the two subgroups were compared through differential expression analysis, and KEGG pathway enrichment of the selected DEGs highlighted their primary roles in immune function and associated diseases like Rheumatoid arthritis and the IL-17 signaling pathway (Figure 2I). In addition, Table 2 summarises the distribution of clinical characteristics of patients with both subgroups, further supporting the existence of significant clinical differences between subtypes.

Development and Validation of Prognostic Models

Prognostic models were developed using genes that differed between subtypes. Initially, univariate Cox regression pinpointed 23 genes that showed a strong association with patient prognosis, meeting the significance criterion of $p < 0.01$ (Figure 3A, Supplementary Table S2). To address multicollinearity and refine the gene set, LASSO regression was applied, narrowing the list down to 13 key prognostic genes (Figure 3B and 3C, Supplementary Table S3). These genes were then subjected to multivariate Cox analysis, which ultimately selected four signature genes—*CXCL1*, *HLA-DRA*, *POSTN*, and *TGFBI*—for constructing the final prognostic model (Figure 3D, Supplementary Table S4). Figure 3E displays the expression patterns of the four key signature genes in tumor versus normal tissues, revealing that *CXCL1*, *HLA-DRA*, and *TGFBI* were markedly elevated in tumor specimens. Based on the prognostic model developed, patients were divided into high-risk and low-risk groups according to their assigned risk scores. Within the TCGA training dataset, the prognostic model demonstrated robust predictive performance, with area under the ROC curve (AUC) values of 0.822, 0.682, and 0.695 for 1-, 3-, and 5-year survival predictions, respectively (Figure 3F). Furthermore, survival analysis showed that individuals categorized as low-risk had notably better survival outcomes than those assigned to the high-risk group (Figure 3G). Figure 3H presents the spread of risk scores in relation to the survival status of the patients, further confirming the model's ability to distinguish between risk groups. To evaluate the reliability of the model, it was tested on the independent GSE52903 dataset, producing findings that aligned closely with those observed in the TCGA training cohort. In this validation group, ROC curve analysis showed AUC values of 0.702, 0.669, and 0.71 for predicting survival at 1, 3, and 5 years, respectively (Figure 3I). Similar to the training data, patients identified as low-risk exhibited significantly better survival rates (Figure 3J). Figure 3K depicts the spread of risk scores in relation to survival outcomes across both high- and low-risk groups, highlighting the model's consistency and dependability. Additionally, expression boxplots comparing the signature genes between risk groups revealed that, with the exception of *HLA-DRA*, the remaining three genes showed significantly higher expression levels in the high-risk group (Figure 3L). Survival analysis conducted on each individual gene revealed that higher expression levels of all four genes were closely associated with

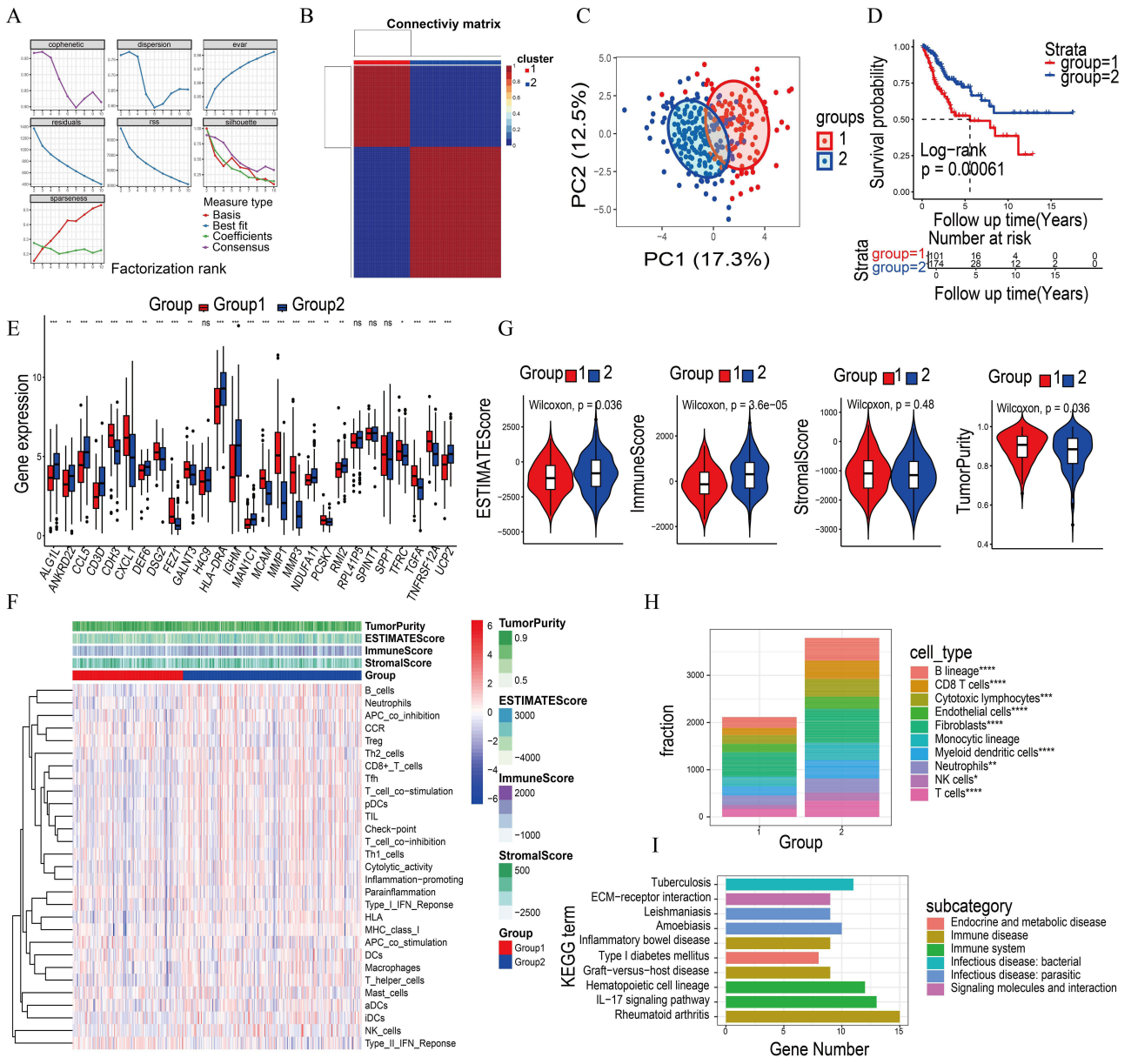

Figure 2 Analysis of NMF clustering and enrichment. (**A**) Clustering of expression profiles for 27 prognostic genes using the NMF method. Red colour represents the baseline. (**B**) NMF heatmap with the number of selected subgroups as 2. (**C**) PCA plot showing the spatial distribution of the two groups of samples. (**D**) K-M survival curve comparison between the group1 and group2. Red colour indicates the first group and blue colour indicates the second group. (**E**) Boxplot of prognostic gene expression. About half of them are highly expressed in group1 and the other half in group2. (**F**) Heatmap depicting differences in immune cell infiltration across the two separate subgroups. (**G**) Comparison of ESTIMATE scores, immune scores, stromal scores, and tumor purity between the different subgroups. (**H**) Evaluation of immune cell infiltration across the subgroups using the MCP-counter method. (**I**) KEGG pathway analysis highlighting enriched signaling routes among genes differentially expressed between the subgroups. Statistical significance: ****, p less than 0.0001; ***, p-value between 0.0001 and 0.001; **, p-value between 0.001 and 0.01; *, p-value ranging from 0.01 to 0.05; and ns denotes non-significant results where p-value exceeds 0.05.

unfavorable patient outcomes (Figure 3M). RT-qPCR experiments confirming the expression patterns of the signature genes (Figure 3N).

Pathway Enrichment Analysis of Different Risk Groups

Next, pathway enrichment analysis was performed on the high- and low-risk groups utilizing GSEA version 4.3.2. Results indicated that the low-risk cohort showed notable enrichment in pathways related to immune system activities, such as antigen recognition, immune memory, immune regulation, and energy metabolism. This suggests that the immune system in the low-risk group operates in a highly coordinated and active manner. Notably, the enrichment of

https://doi.org/10.2147/IJWH.S537092

Table 2 Summary of Clinical Characteristics Among Subgroups

Name	Levels	Group1 (N=109)	Group2 (N=184)	P value
OS	0	70 (64.2%)	150 (81.5%)	0.002
	1	39 (35.8%)	34 (18.5%)	
Age	Mean ± SD	45.4 ± 13.7	49.6 ± 13.7	0.013
Grade	G1	6 (5.5%)	13 (7.1%)	0.840
	G2	46 (42.2%)	83 (45.1%)	
	G3	47 (43.1%)	70 (38%)	
	G4	0 (0%)	1 (0.5%)	
	Unknown	10 (9.2%)	17 (9.2%)	
Stage	Stage I	57 (52.3%)	100 (54.3%)	0.687
	Stage II	22 (20.2%)	42 (22.8%)	
	Stage III	19 (17.4%)	23 (12.5%)	
	Stage IIV	7 (6.4%)	15 (8.2%)	
	Unknown	4 (3.7%)	4 (2.2%)	
T	T1	53 (48.6%)	84 (45.7%)	0.030
	T2	15 (13.8%)	53 (28.8%)	
	T3	7 (6.4%)	10 (5.4%)	
	T4	4 (3.7%)	6 (3.3%)	
	Unknown	30 (27.5%)	31 (16.8%)	
N	N0	43 (39.4%)	86 (46.7%)	0.329
	N1	20 (18.3%)	36 (19.6%)	
	Unknown	46 (42.2%)	62 (33.7%)	
M	M0	34 (31.2%)	73 (39.7%)	0.226
	M1	3 (2.8%)	8 (4.3%)	
	Unknown	72 (66.1%)	103 (56%)	

pathways involved in immunological memory indicates that individuals in the low-risk group may possess enhanced immune surveillance and responsiveness (Figure 4A). Conversely, the high-risk group was predominantly enriched in pathways involved in cell growth, tissue restructuring, and the formation of new blood vessels. These findings indicate that tumor cells in high-risk patients possess enhanced growth and invasive capabilities. For example, pathways related to the suppression of cell-matrix adhesion and the enhancement of nuclear division (Figure 4B) were significantly enriched, indicating major changes in cell adhesion mechanisms and cell cycle regulation that likely contribute to tumor growth and metastatic potential within this group. We further explored the functions of DEGs between high- and low-risk groups through GO and KEGG enrichment analyses. GO biological process enrichment indicated a heightened state of foreign antigen processing and presentation within the adaptive immune system. Pathways associated with MHC protein complex assembly and the processing/presentation of foreign antigens were particularly enriched (Figure 4C). This suggests a robust immune response activation related to antigen presentation in these groups. KEGG pathway analysis demonstrated that the DEGs were predominantly linked to immune-related disorders and immune system activities, encompassing pathways such as hematopoietic cell lineage, rheumatoid arthritis, as well as other autoimmune and chronic inflammatory diseases (Figure 4D). This further supports the significant role of the immune system in determining disease prognosis.

Construction of Nomogram

To evaluate how risk scores influence patient outcomes, we integrated risk scores with clinical variables in both univariate and multivariate Cox regression analyses (Figure 5A and B). The findings indicated that risk score and patient age are likely key determinants of prognosis. We then created a nomogram integrating risk score, age, disease stage, and TN staging to predict survival outcomes at 1, 3, and 5 years for patients (Figure 5C). The DCA curve indicated that this model offered a high net clinical advantage within certain threshold limits (Figure 5D). The calibration curve additionally validates the strong agreement between survival probabilities estimated by the nomogram and the observed patient survival outcomes (Figure 5E).

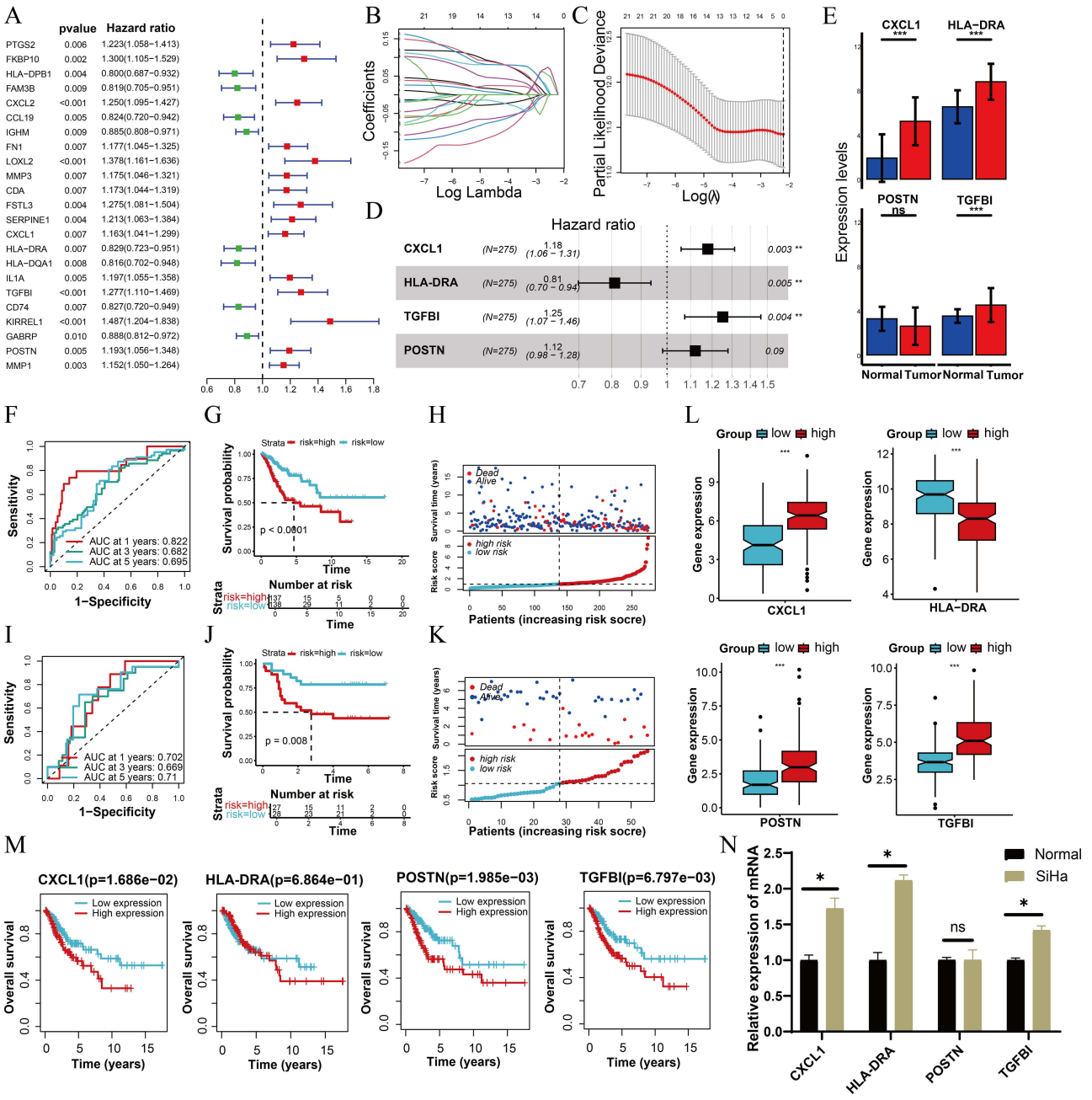

Figure 3 Identification and modeling of prognostic signature genes in CC. (**A**) Forest plot displaying results from univariate Cox regression for 23 genes associated with prognosis. (**B**) Distribution plot and (**C**) coefficient spectrum of log(β) sequences in LASSO regression model. (**D**) Forest plot summarizing multivariate Cox analysis of four key prognostic genes. (**E**) Boxplots illustrating the differential expression of signature genes in cervical cancer versus normal tissue samples. (**F**) ROC curves assessing the prognostic gene signature's ability to predict outcomes (**G**) K-M survival curves comparing survival probabilities between patients categorized into high-risk and low-risk groups. (**H**) Scatterplot of the distribution of patient survival versus risk score. (**I**) ROC curves illustrating the accuracy of 1-, 3-, and 5-year overall survival predictions within the GSE52903 cohort. (**J**) K-M survival analysis comparing patient groups within the GSE52903 cohort. (**K**) Scatterplot showing patient survival status in relation to risk scores in the GSE52903 cohort. (**L**) Boxplots illustrating expression differences of signature genes between different risk groups. (**M**) K-M analysis of signature genes. (**N**) RT-qPCR results of signature genes. Statistical significance: ***, p-value below 0.001; **, p-value between 0.001 and 0.01; *, p-value ranging from 0.01 to 0.05; and ns denotes non-significant results where p-value exceeds 0.05.

Subgroup Analysis of Risk Scores and Clinical Characteristics in CC Patients

We also analyzed how clinical features were distributed among patients classified into different risk groups (Supplementary Figure S2A). Patients were categorized into subgroups according to various clinical parameters, including age (≤65 versus >65), tumor grade (G1 compared to G2-4), overall disease stage (Stage I and II versus

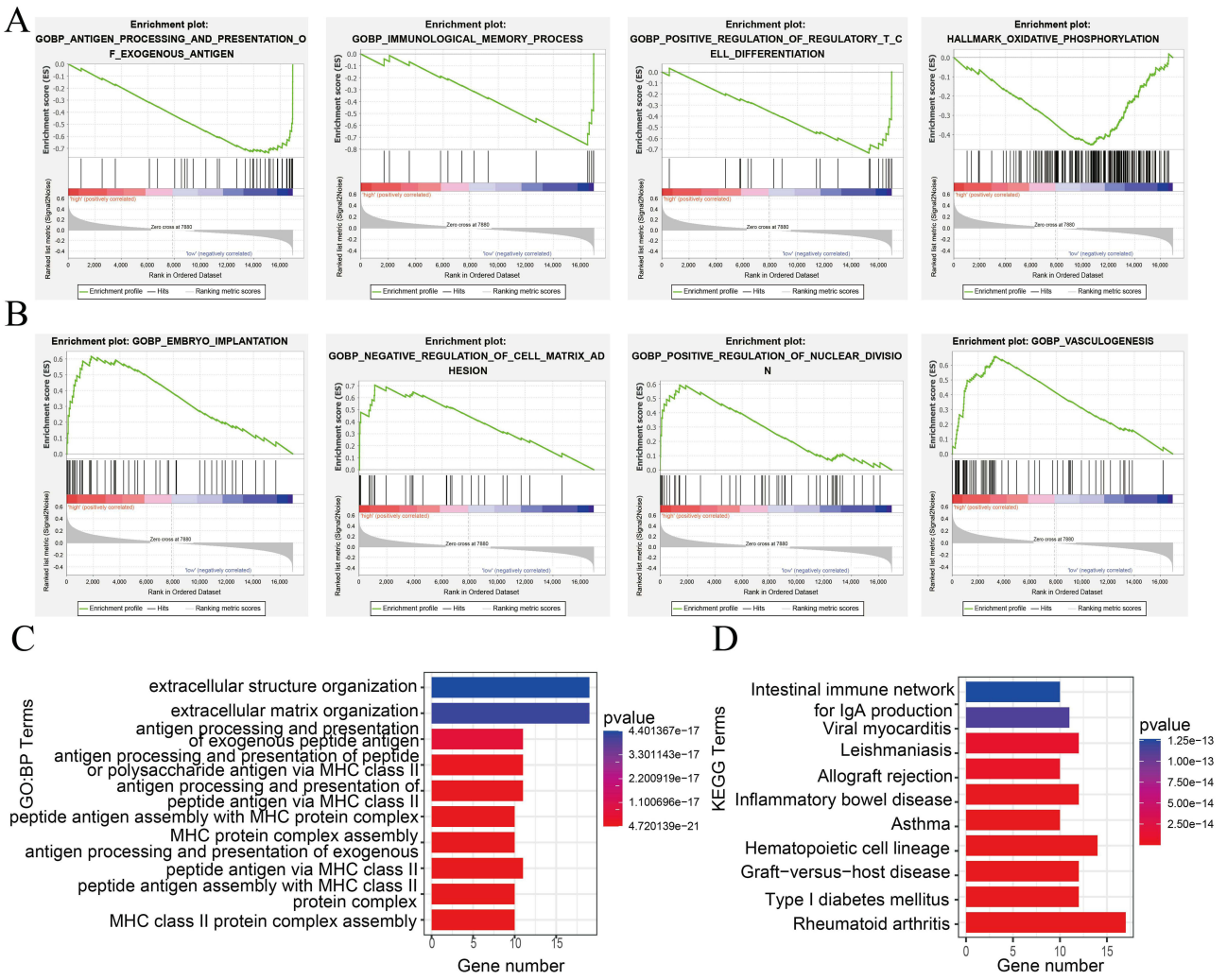

Figure 4 GSEA and DEGs enrichment analyses comparing different risk groups. (**A**) GSEA results highlighting pathways prominently enriched in the low-risk cohort. (**B**) GSEA findings showing pathways significantly enriched within the high-risk cohort. (**C**) GO biological process enrichment analysis of DEGs distinguishing the two risk groups. (**D**) KEGG pathway enrichment of DEGs distinguishing the two groups. BP: biological process.

Stage III and IV), T classification (T1 and T2 versus T3 and T4), N classification (N0 versus N1), and M classification (M0 versus M1). K-M survival analyses within these subgroups consistently showed that patients classified as high-risk had markedly worse overall survival outcomes than those in the low-risk category (Supplementary Figure S2B).

Analysis of Immune Cell Infiltration and Forecasting of Immunotherapy Outcomes

To uncover the distinct immune profiles between different risk groups of patients, we performed a systematic assessment using a variety of immune-related analyses. We revealed significant variations in the infiltration levels of 10 immune cell types as well as differences in 9 immune-related functional pathways when comparing the high-risk and low-risk groups using ssGSEA (Figure 6A and B), indicating distinct immune microenvironmental characteristics. Further analysis utilizing the CIBERSORT algorithm uncovered notable differences in the infiltration levels of several immune cell types, including CD8+ T cells, resting CD4+ memory T cells, M0 and M1 macrophages, activated dendritic cells, and activated mast cells between the different risk groups (Figure 6C). In addition, examination of immune checkpoint gene expression revealed that most of these genes exhibited significant differential expression between the two risk categories (Figure 6D). Furthermore, Pearson correlation analysis indicated a strong relationship between the expression of the signature genes and the degree of immune cell infiltration (Figure 6E). Building on the immune infiltration assessment, we further investigated the potential link between risk groups and immunotherapy responsiveness. The comparison of

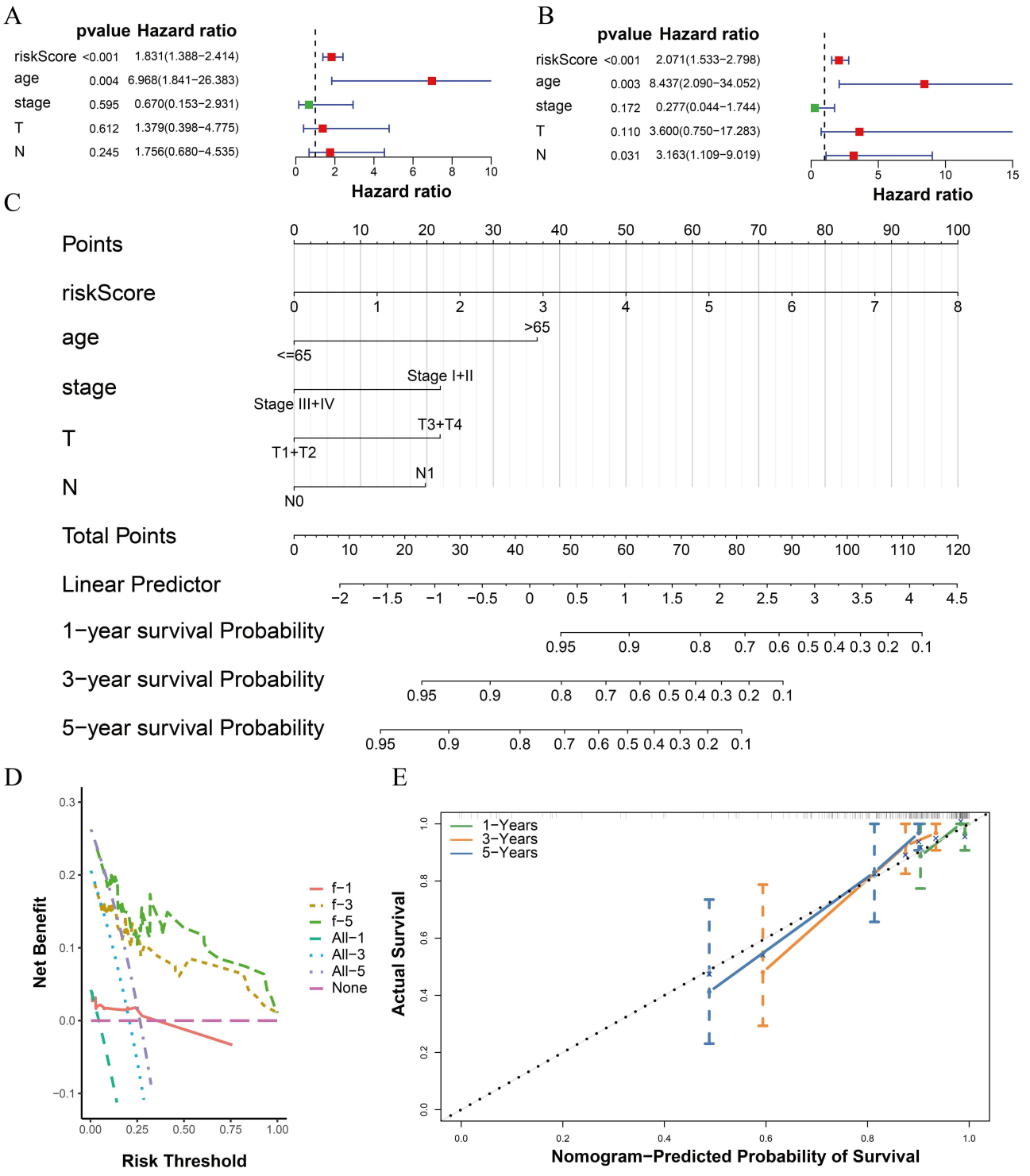

Figure 5 Construction of nomogram. (**A**) Univariate Cox regression analysis. (**B**) Multivariate Cox regression analysis. (**C**) Nomogram constructed based on risk scores versus clinical characteristics. (**D**) DCA curve analysis of the nomogram. The vertical coordinate represents the net benefit and assesses the value of clinical application of the nomogram at different thresholds. (**E**) Calibration curves for the nomogram.

IPS values showed that individuals classified as low-risk exhibited significantly elevated IPS scores relative to those in the high-risk group, suggesting that the low-risk patients may have a more favorable response to immunotherapy (Figure 6F). To further assess the ability of risk scores to predict immunotherapy outcomes, we examined data from the IMvigor210 cohort, which includes patients who received PD-L1 inhibitor treatment. Survival analysis demonstrated

https://doi.org/10.2147/IJWH.S537092

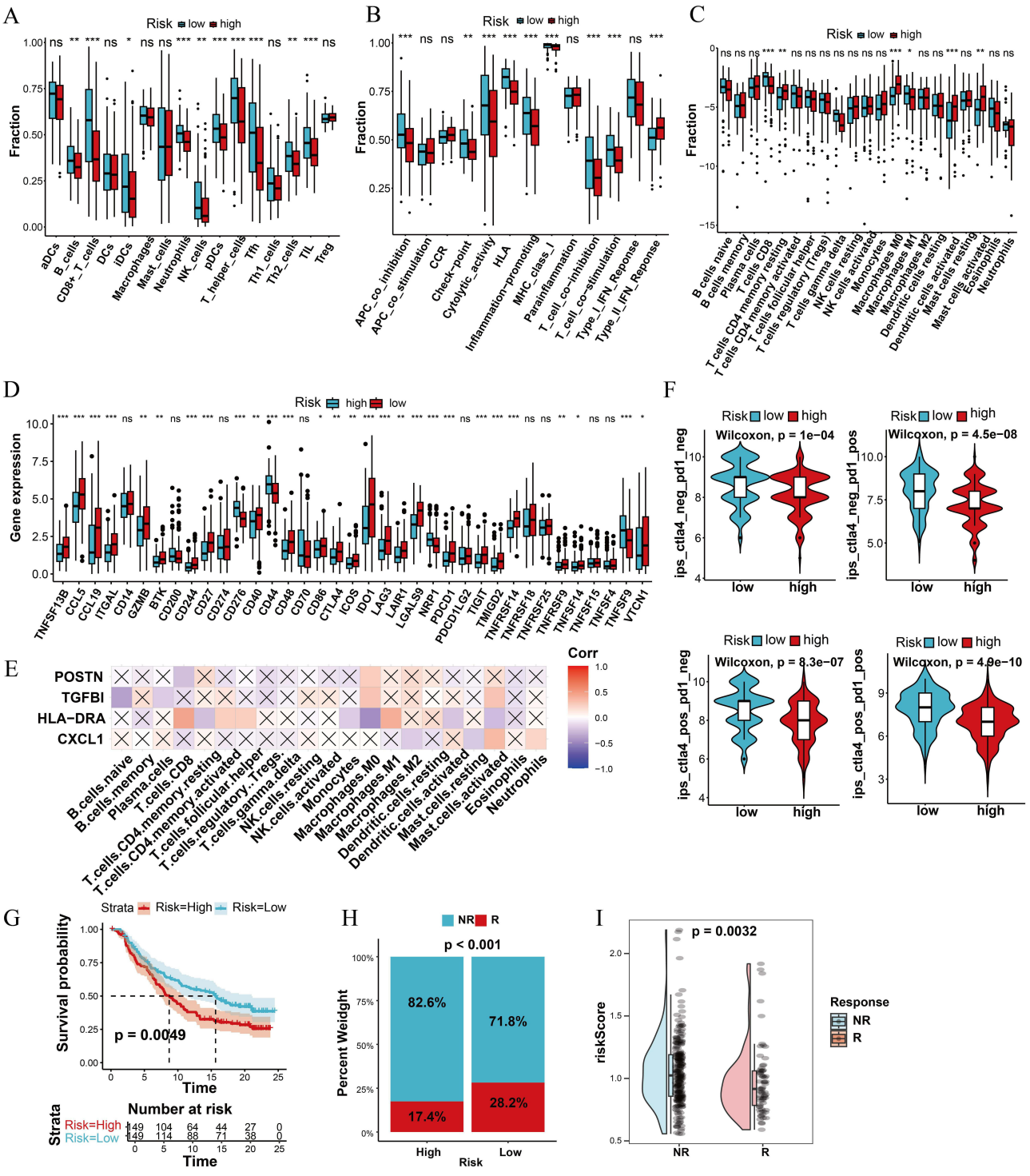

Figure 6 Analysis of immune features and immunotherapy response in patients stratified by risk groups. (**A**) Boxplots illustrating ssGSEA-derived immune cell scores comparing different risk groups. (**B**) Boxplots showing ssGSEA immune function scores across the two risk categories. (**C**) Immune cell infiltration differences between different risk groups assessed by the CIBERSORT algorithm. (**D**) Comparative expression analysis of immune checkpoint genes in different risk groups of patients. (**E**) Heatmap illustrating the relationships between the expression of signature genes and the extent of immune cell infiltration. (**F**) Comparison of IPS values between different risk groups. (**G**) K-M survival curves of the IMvigor210 cohort. (**H**) Distribution of immunotherapy responders (**R**) and non-responders (NR) within the two risk categories. Blue represents NR and red represents R. (**I**) Comparison of risk scores between patients who responded to immunotherapy (**R**) and those who did not (NR). Statistical significance: ***, p-value below 0.001; **, p-value between 0.001 and 0.01; *, p-value ranging from 0.01 to 0.05; and ns denotes non-significant results where p-value exceeds 0.05.

that patients in the low-risk category had markedly better survival outcomes than those assigned to the high-risk group (Figure 6G). Moreover, the low-risk cohort showed a significantly greater proportion of favorable responses to immunotherapy compared to the high-risk cohort (Figure 6H). Furthermore, individuals who showed a positive response to immunotherapy exhibited notably reduced risk scores compared to those who did not respond (Figure 6I), suggesting that lower risk scores could be linked to more favorable treatment results.

TMB and Drug Sensitivity Analysis

To explore the mutation landscape of patients stratified by risk, we conducted an analysis of TMB. The results indicated that the *TTN* gene mutation occurred slightly more often in the low-risk group than in the high-risk group, with frequencies of 17% versus 15%, respectively (Figure 7A and B). Moreover, patients in the high-risk category exhibited a reduced overall TMB compared to their low-risk counterparts (Figure 7C). To assess variations in chemotherapy

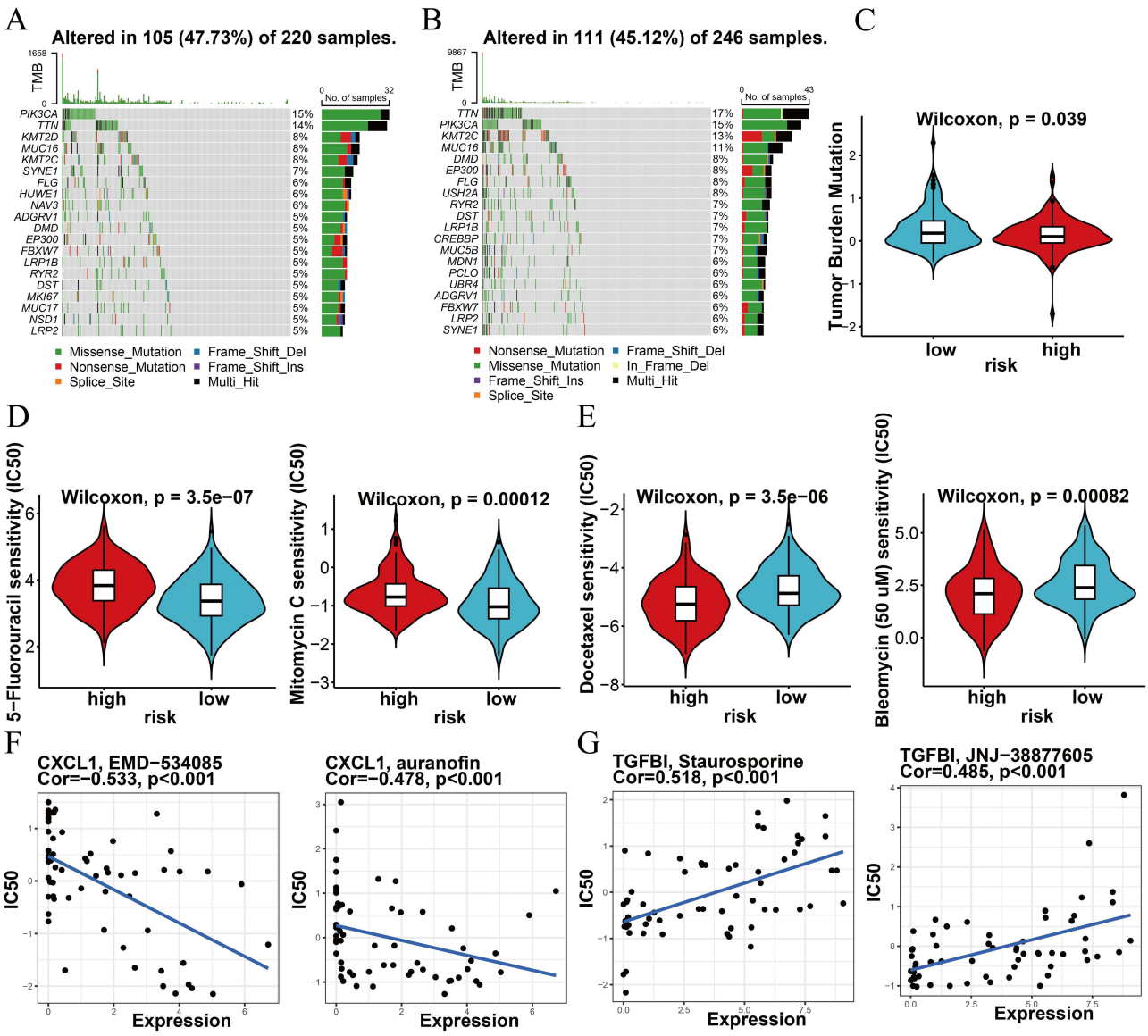

Figure 7 Mutation profiles and drug sensitivity analyses of patients in different risk groups. (**A**) Mutation waterfall plot of the high-risk group (top20). (**B**) Mutation waterfall plot of the low-risk group (top20). (**C**) Comparative analysis of TMB between the two groups. (**D**) Comparison of 5-fluorouracil and mitomycin C IC50 values between different risk groups. (**E**) IC50 values for docetaxel and bleomycin (50 μM) compared across different risk groups. (**F**) Analysis of how *CXCL1* expression correlates with drug sensitivity. *CXCL1* expression was positively correlated with EMD-534085 and auranofin. (**G**) Relationship between *TGFBI* expression level and drug sensitivity. *TGFBI* expression was negatively correlated with Sepantronium and JNJ-38877605.

https://doi.org/10.2147/IJWH.S537092

responsiveness between the different risk groups, the pRRophetic algorithm was utilized to predict IC50 values for four drugs frequently administered in CC treatment. The results indicated that patients categorized as low-risk exhibited increased sensitivity to 5-fluorouracil and mitomycin C (Figure 7D), whereas those in the high-risk group were more susceptible to docetaxel and bleomycin (at 50 μM) (Figure 7E). Additionally, using the CellMiner database, correlation analysis revealed a significant negative relationship between *CXCL1* expression and the IC50 values of EMD-534085 and auranofin (Figure 7F, Supplementary Table S5). Conversely, *TGFBI* expression showed a positive correlation with the IC50 values of Sepantronium and JNJ-38877605 (Figure 7G, Supplementary Table S5). In contrast, *TGFBI* expression was positively correlated with the IC50 values for Sepantronium and JNJ-38877605 (Figure 7G, Supplementary Table S5).

Construction of TF and miRNA Network Related to Characteristic Genes

In addition, we predicted 30 miRNAs (eg miR-98-5p, miR-30a-5p) and 26 TFs (eg *FOXC1*) upstream of the characterised genes (*CXCL1*, *HLA-DRA*, *POSTN*, and *TGFBI*). The complete regulatory network was shown in Supplementary Figure S3.

Discussion

LPS, a potent immunostimulant, is pivotal in the development of CC and influences the TME.[36] In this study, based on the molecular subtypes identified by bacterial LRGs, we constructed a risk model containing four characteristic genes, providing a new molecular tool for the prognostic assessment of CC patients. The model successfully separated patients into different risk categories, with those in the low-risk group exhibiting markedly improved prognosis. Compared to the patients in the high-risk group, low-risk patients demonstrated longer survival, greater immune cell infiltration, and enhanced responsiveness to immunotherapy. In addition, we evaluated variations in chemotherapy drug sensitivity across risk groups, suggesting that the model not only has prognostic value, but may also guide the development of individualised treatment regimens and improve the efficacy of immunotherapy and targeted therapies. The functional enrichment results indicated that the LRGs with altered expression in CC predominantly participate in mediating cell adhesion and chemokine functions, highlighting their significance in maintaining tight connections between cells and the extracellular matrix. Moreover, these genes influence the recruitment and positioning of immune cells, playing a critical role in immune cell infiltration and the overall immune response in CC.[40–42] Further analysis of biological processes and cellular components revealed that these genes are participate in the regulation of epithelial cell development, extracellular matrix organisation and adhesion junction structures, suggesting that they may influence the role of tumour-associated myofibroblasts (myCAFs) in the remodelling of the microenvironment of CC, which in turn promotes tumour cell proliferation and metastasis.[8,43] In addition, KEGG pathway enrichment emphasises the activation of cell cycle and cytoskeletal regulatory pathways, which to some extent reflects the dynamic changes of CC cells in proliferation and migration. It has been previously shown that lipopolysaccharide signalling in the TME may influence immune escape and therapeutic response in CC by regulating immune cell function and extracellular matrix remodelling.[44–46] In summary, LRGs not only reveal the complex regulatory mechanisms of the TME in CC, but also provide potential molecular targets and theoretical basis for targeting the TME and improving the efficacy of immunotherapy.

Our study first identified two molecular subtypes associated with LPS and they differed significantly in prognosis. Group 2 had better survival, higher levels of immune cell infiltration and a relatively active immune microenvironment. Differential genes between the two subtypes mainly focused on disease- and immune-related pathways, such as Rheumatoid arthritis and IL-17 signaling pathway, suggesting that LPS may affect tumour immune escape and patient prognosis by modulating immune responses. This finding not only deepens the understanding of the heterogeneity of the tumour immune microenvironment, but also enhances our understanding of the immunomodulatory role of LPS.

Our study identified four key prognostic genes (*CXCL1*, *HLA-DRA*, *POSTN*, and *TGFBI*), which are characteristically closely associated with the onset and progression of CC. *CXCL1*, a CXC chemokine, has been shown to play pro-inflammatory and immunomodulatory roles in a variety of tumours.[47,48] *CXCL1* in CC may promote tumour progression and metastasis by modulating the recruitment of immune cells with the inflammatory state of the TME.[49,50] These chemokine profiles have previously been suggested to serve as biomarkers for the detection of cervical precancerous

lesions.[51,52] Previously, it has been shown that monoclonal antibodies targeting *CXCL1* (eg HL2401) display inhibitory effects on tumour cell proliferation, invasion and angiogenesis in vitro and in animal models, significantly delaying tumour growth in bladder and prostate cancers.[53] Our research revealed elevated *CXCL1* expression in CC and among high-risk patients, aligning with earlier findings that link high *CXCL1* levels to unfavorable CC prognosis.[54–57] As a crucial part of MHC class II molecules, *HLA-DRA* plays an important role, is participates in antigen presentation and activates CD4+ T cells, which in turn affects tumour immunosurveillance.[58] *HLA-DRA* has been shown to serve as a prognostic marker for clinical outcomes.[59,60] Our research revealed that *HLA-DRA* expression is elevated in CC and correlates with unfavorable prognosis. Notably, however, *HLA-DRA* levels were lower in the high-risk group, suggesting a potential involvement of specific mechanisms governing *HLA-DRA* function throughout disease progression. This complex dynamic may be related to the different stages of immune escape from the tumour. On the one hand, high *HLA-DRA* expression reflects active inflammation and immune activation in the TME.[61] However, certain immunosuppressive cells such as tumour-associated macrophages (TAMs) also express *HLA-DRA*, which induces immune tolerance through the presentation of self-antigens or inhibitory molecules, promotes tumour progression and leads to a poor prognosis.[62,63] On the other hand, decreased *HLA-DRA* expression in the high-risk group may be a mechanism by which tumour cells evade immune surveillance. With disease progression, tumours down-regulate MHC II expression through epigenetic modifications, immunosuppressive factors (eg, TGF-β, IL-10), or HPV infection, which attenuates antigen-presenting ability and helps to evade recognition by CD4+ T cells, and ultimately leads to a poor prognosis.[64] Previous studies have also indicated that *HLA-DRA* could be a potential target for anti-tumour therapy in CC.[65] The specific expression patterns of *HLA-DRA* in different cell types (eg tumour cells, antigen-presenting cells, etc.) need to be investigated in more depth in the future. Bone bridging protein (POSTN), an extracellular matrix protein involved in cell adhesion, migration and remodelling of the TME, promotes tumour cell invasion and metastasis, and has been identified as a marker of poor prognosis in a variety of cancers.[66–68] A previous study indicated that high expression of *POSTN* in CC was a risk factor for poor prognosis in CC patients undergoing radical radiotherapy.[69] In a mouse trial, POSTN pathway blockade combined with PD-L1 inhibitor treatment was found to significantly inhibit tumour growth and alter the immune cell composition of the TME.[70] Our findings revealed that *POSTN* expression was elevated in the high-risk group and strongly correlated with unfavorable prognosis. Transforming growth factor β-inducible protein (TGFBI) is a key regulatory molecule mainly distributed in the extracellular matrix, it modulates diverse biological activities, including cell proliferation, differentiation, and migration by interacting with cell surface receptors and extracellular matrix components, and its aberrant expression is closely related to tumour invasiveness and drug resistance.[71–73] One study indicated that down-regulation of *TGFBI* could make CC cells more sensitive to cisplatin.[74] These findings imply that *TGFBI* could be a key factor contributing to chemoresistance in CC. Our research revealed that *TGFBI* expression was markedly elevated in CC and among patients classified as high-risk. Taken together, these four genes not only play important roles in regulating the biological behaviour of CC cells, but may also serve as potential prognostic markers and therapeutic targets by impacting the TME and extracellular matrix dynamics.

The TME in CC patients is characterized by significant heterogeneity and disrupted immune regulation.[6,7,23] Analysis of immune cell infiltration revealed that individuals classified as low-risk demonstrated a more robust anti-tumor immune environment, characterized by notably increased infiltration of CD8+ T cells and M1 macrophages, which correlated strongly with improved responses to immunotherapy and favorable survival outcomes. CD8+ T cells directly killed tumour cells by secreting granzyme B and perforin,[75–78] while M1 macrophages activate the Th1-type immune response by releasing IL-12 and TNF-α, which together constitute the core effector mechanism of anti-tumour immunity.[79,80] In contrast, patients classified as high-risk often display an immature immune microenvironment, characterized by the presence of resting CD4+ memory T cells and M0 macrophages, which may contribute to immune evasion and diminished effectiveness of immunotherapy.[81,82] The prediction of response to immunotherapy further revealed differences in the immune microenvironment across risk groups. Specifically, low-risk patients exhibited higher IPS scores, suggesting a more active immune system and anti-tumour potential. High IPS values typically correspond to increased immune cell infiltration and more potent immune effector functions in the TME, supporting a favorable response to therapies targeting immune checkpoints like anti-PD-L1 antibodies.[83,84] Our findings showed that individuals classified as low-risk exhibited notably greater response rates to anti-PD-L1 treatment compared to those in the high-risk category.

Moreover, correlation analyses between signature genes and immune cell infiltration levels highlighted the crucial role these genes play in immune regulation, especially concerning M0 macrophages and activated mast cells.

Further TMB analysis showed that the overall TMB was higher in the low-risk group than in the high-risk group. This finding is consistent with previous studies that high TMB is usually positively correlated with immunotherapy response, as higher mutation loads generate more neoantigens and enhance tumour immunogenicity, thereby activating the body's anti-tumour immune response.[85] It has also been shown that patients with high TMB have better outcomes when treated with immune checkpoint inhibitors, with significantly longer objective remission rates and progression-free survival.[86] In addition, we observed a significant increase in the mutation frequency of the *TTN* gene in the low-risk group. *TTN*, as a common high-volume mutated gene, has the potential for its variation to contribute to the generation of neoantigens and further activate the immune response, thus providing a molecular basis for the good prognosis of the low-risk group.[87,88] These findings highlight the critical role of TMB and specific gene variants in regulating the TME, suggesting that future studies could delve into the complex relationship between TMB and immune infiltration and the differences in immunogenicity of different mutant genes to optimise immunotherapeutic strategies.

Finally, a sensitivity prediction analysis for various chemotherapeutic agents was carried out across high- and low-risk groups, demonstrating greater susceptibility to 5-fluorouracil and mitomycin C in the low-risk patients. This could be attributed to the lower proliferative capacity of tumor cells within the low-risk group, their weaker DNA repair capacity, and a more active immune microenvironment, which rendered these cells more susceptible to the killing effects of antimetabolite and antimicrotubule drugs.[89–91] On the contrary, patients classified as high-risk showed greater sensitivity to docetaxel and bleomycin, suggesting that tumor cells in this group might rely on different biological pathways to make them more sensitive to these drugs, such as cell cycle control and DNA damage repair.[92–95] Such differences reflect the heterogeneity of molecular features and drug action mechanisms in tumours of different risk groups, providing an important basis for the design of clinical individualized chemotherapy regimens. It should be noted that drug sensitivity analyses rely only on computational prediction, with certain uncertainty in the results, and lack of in vitro or clinical experimental support. Therefore, these results are only for preliminary reference at present, and it is necessary to further validate their reliability through multi-centre clinical samples or cell/animal experiments in the future to enhance the practical application value.

In conclusion, our study successfully identified 2 bacterial LPS-associated molecular subtypes and developed a risk model capable of accurately forecasting patient outcomes. Compared with traditional prognostic models, it has certain advantages. Existing prognostic models based on core EMT genes (eg, *VIM*, *CDH2*) mainly predict the risk of tumour metastasis, reflecting the migratory and invasive ability of tumour cells, but they are insufficient in explaining the role of the regulation of the immune microenvironment in early-stage CC, and are difficult to reveal the mechanisms of immune cell infiltration and immune escape.[96] Meanwhile, existing HPV-associated models only apply to HPV-positive patients and rely on E6/E7 expression, neglecting the role of HPV-negative patients and microbial factors such as LPS in tumour immune escape.[97,98] In contrast, the prognostic model constructed based on LPS in this study highlights the tumour immune microenvironment and microbe-tumour interactions, which not only predicts excellent survival, but also focuses on key immune pathways, providing new potential targets for immune microenvironment-related therapies, and expanding the scope of existing models. However, there are limitations to this study. Firstly, the data utilized were sourced from public databases, and future studies need more external datasets as well as clinical cohorts for validation. Secondly, our study only offered a preliminary insight into the roles of the identified signature genes in CC, and the specific biological mechanisms behind them remain to be elucidated. Network analysis of miRNAs and TFs upstream of the signature genes can further narrow down the scope for future studies (Supplementary Figure S3). Finally, due to the limitation of time and experimental conditions, RT-qPCR was only performed in one CC cell line at present, and will be extended to multiple cell lines or clinical samples for further validation in the future. In addition, since our study primarily relied on bioinformatics approaches, we failed to further verify the specific regulatory roles of LPS and LRGs in the CC TME through in vitro cellular experiments. Subsequent experimental confirmation at the molecular mechanism level can be performed in combination with cellular and animal models to enhance the persuasiveness of the study conclusions. The imperfect clinical information (eg, HPV typing, etc.) in public databases may affect the results of the analyses, and it is necessary to conduct in-depth studies based on large samples and complete clinical information in the future, especially

the comparative analyses of different subgroups of HPV. Nevertheless, our study still provide new perspectives for understanding the mechanism of bacterial LPS in tumour immunity, which has important clinical translational value.

Conclusion

Overall, we developed a risk model capable of accurately forecasting the prognosis of CC patients. Four CC-related prognostic biomarkers were identified, revealing their important roles in intercellular adhesion and immune regulation, which provided a theoretical basis for an in-depth understanding of the TME and LPS-mediated tumour mechanisms in CC, and provided new perspectives on immunotherapy and individualised chemotherapeutic strategies for CC.

Data Sharing Statement

The data and materials in the current study are available from the corresponding author on reasonable request.

Ethics Approval and Consent to Participate

This study was carried out in strict accordance with the ethical guidelines of the Declaration of Helsinki II. It has been reviewed and approved by the Medical Ethics Committee of Jinhua Central Hospital, with the approval number (20251980101). It has also obtained the approval document from the Medical Ethics Committee of Jinhua Maternal and Child Health Care Hospital (Approval Number: 2025KY043).

Author Contributions

All authors made a significant contribution to the work reported, whether that is in the conception, study design, execution, acquisition of data, analysis and interpretation, or in all these areas; took part in drafting, revising or critically reviewing the article; gave final approval of the version to be published; have agreed on the journal to which the article has been submitted; and agree to be accountable for all aspects of the work.

Funding

This study was supported by the Jinhua Science and Technology Plan Project – Key Projects in Social Development (Grant No. 2023-3-153), entitled ‘Correlation between Cervical Injury and Regeneration after LEEP Surgery and the Vaginal Microecology.

Disclosure

The authors declare that they have no potential conflicts of interest. This manuscript was previously uploaded as a preprint on ResearchSquare (DOI: https://www.researchsquare.com/article/rs-6533637/v1).

References

1. Siegel RL, Miller KD, Jemal A. Cancer statistics, 2018. *Ca a Cancer J Clin*. 2018;68(1):7–30. doi:10.3322/caac.21442
2. Bray F, Laversanne M, Sung H, et al. Global cancer statistics 2022: GLOBOCAN estimates of incidence and mortality worldwide for 36 cancers in 185 countries. *Ca a Cancer J Clin*. 2024;74(3):229–263. doi:10.3322/caac.21834
3. Singh D, Vignat J, Lorenzoni V, et al. Global estimates of incidence and mortality of cervical cancer in 2020: a baseline analysis of the WHO global cervical cancer elimination initiative. *Lancet Glob Health*. 2023;11(2):e197–e206. doi:10.1016/S2214-109X(22)00501-0
4. Marth C, Landoni F, Mahner S, et al. Cervical cancer: ESMO clinical practice guidelines for diagnosis, treatment and follow-up. *Ann Oncol*. 2017;28 (suppl_4):iv72–iv83. doi:10.1093/annonc/mdx220
5. Guimarães YM, Godoy LR, Longatto-Filho A, et al. Management of early-stage cervical cancer: a literature review. *Cancers*. 2022;14(3):575. doi:10.3390/cancers14030575
6. Cao G, Yue J, Ruan Y, et al. Single-cell dissection of cervical cancer reveals key subsets of the tumor immune microenvironment. *EMBO J*. 2023;42 (16):e110757. doi:10.15252/embj.2022110757
7. Yuan Y, Cai X, Shen F, et al. HPV post-infection microenvironment and cervical cancer. *Cancer Letters*. 2021;497:243–254. doi:10.1016/j.canlet.2020.10.034
8. Ou Z, Lin S, Qiu J, et al. Single-nucleus RNA sequencing and spatial transcriptomics reveal the immunological microenvironment of cervical squamous cell carcinoma. *Adv Sci*. 2022;9(29):e2203040. doi:10.1002/advs.202203040
9. Li C, Wu H, Guo L, et al. Single-cell transcriptomics reveals cellular heterogeneity and molecular stratification of cervical cancer. *Commun Biolog*. 2022;5(1):1208. doi:10.1038/s42003-022-04142-w

10. Xiao Y, Yu D. Tumor microenvironment as a therapeutic target in cancer. *Pharmacol Ther*. 2021;221:107753. doi:10.1016/j.pharmthera.2020.107753
11. Wu T, Dai Y. Tumor microenvironment and therapeutic response. *Cancer Letters*. 2017;387:61–68. doi:10.1016/j.canlet.2016.01.043
12. Tang T, Huang X, Zhang G, et al. Advantages of targeting the tumor immune microenvironment over blocking immune checkpoint in cancer immunotherapy. *Signal Transd Targeted Therapy*. 2021;6(1):72.
13. Anderson NM, Simon MC. The tumor microenvironment. *Curr Biol*. 2020;30(16):R921–r925. doi:10.1016/j.cub.2020.06.081
14. Mao X, Xu J, Wang W, et al. Crosstalk between cancer-associated fibroblasts and immune cells in the tumor microenvironment: new findings and future perspectives. *Mol Cancer*. 2021;20(1):131. doi:10.1186/s12943-021-01428-1
15. Gajewski TF, Schreiber H, Fu YX. Innate and adaptive immune cells in the tumor microenvironment. *Nat Immunol*. 2013;14(10):1014–1022. doi:10.1038/ni.2703
16. Denk D, Greten FR. Inflammation: the incubator of the tumor microenvironment. *Trends Cancer*. 2022;8(11):901–914. doi:10.1016/j.trecan.2022.07.002
17. McLaughlin M, Patin EC, Pedersen M, et al. Inflammatory microenvironment remodelling by tumour cells after radiotherapy. *Nature Rev Cancer*. 2020;20(4):203–217.
18. Franco EL, Rohan TE, Villa LL. Epidemiologic evidence and human papillomavirus infection as a necessary cause of cervical cancer. *J Nat Cancer Instit*. 1999;91(6):506–511. doi:10.1093/jnci/91.6.506
19. Wei F, Georges D, Man I, et al. Causal attribution of human papillomavirus genotypes to invasive cervical cancer worldwide: a systematic analysis of the global literature. *Lancet*. 2024;404(10451):435–444.
20. Graham SV. The human papillomavirus replication cycle, and its links to cancer progression: a comprehensive review. *Clin Sci*. 2017;131(17):2201–2221. doi:10.1042/CS20160786
21. Westrich JA, Warren CJ, Pyeon D. Evasion of host immune defenses by human papillomavirus. *Virus Research*. 2017;231:21–33. doi:10.1016/j.virusres.2016.11.023
22. Martinelli C, Ercoli A, Parisi S, et al. Molecular mechanisms and clinical divergences in hpv-positive cervical vs. Oropharyngeal cancers: a critical narrative review. *BMC Med*. 2025;23(1):405. doi:10.1186/s12916-025-04247-z
23. Shamseddine AA, Burman B, Lee NY, et al. Tumor immunity and immunotherapy for HPV-related cancers. *Cancer Discov*. 2021;11(8):1896–1912. doi:10.1158/2159-8290.CD-20-1760
24. Ge J, Meng Y, Guo J, et al. Human papillomavirus-encoded circular RNA circE7 promotes immune evasion in head and neck squamous cell carcinoma. *Nat Commun*. 2024;15(1):8609. doi:10.1038/s41467-024-52981-4
25. Maldonado RF, Sá-Correia I, Valvano MA. Lipopolysaccharide modification in gram-negative bacteria during chronic infection. *FEMS Microbiol Rev*. 2016;40(4):480–493. doi:10.1093/femsre/fuw007
26. Whitfield C, Trent MS. Biosynthesis and export of bacterial lipopolysaccharides. *Annu Rev Biochem*. 2014;83(1):99–128. doi:10.1146/annurev-biochem-060713-035600
27. Garcia-Vello P, Di Lorenzo F, Zucchetta D, et al. Lipopolysaccharide lipid A: a promising molecule for new immunity-based therapies and antibiotics. *Pharmacol Ther*. 2022;230:107970. doi:10.1016/j.pharmthera.2021.107970
28. Park BS, Song DH, Kim HM, et al. The structural basis of lipopolysaccharide recognition by the TLR4-MD-2 complex. *Nature*. 2009;458(7242):1191–1195. doi:10.1038/nature07830
29. Park BS, Lee JO. Recognition of lipopolysaccharide pattern by TLR4 complexes. *Exp Mol Med*. 2013;45(12):e66. doi:10.1038/emm.2013.97
30. Ma L, Feng L, Ding X, et al. Effect of TLR4 on the growth of SiHa human cervical cancer cells via the MyD88-TRAF6-TAK1 and NF-κB-cyclin D1-STAT3 signaling pathways. *Oncology Letters*. 2018;15(3):3965–3970. doi:10.3892/ol.2018.7801
31. Jiang N, Xie F, Guo Q, et al. Toll-like receptor 4 promotes proliferation and apoptosis resistance in human papillomavirus-related cervical cancer cells through the Toll-like receptor 4/nuclear factor-κB pathway. *Tumour Biolog*. 2017;39(6):1010428317710586. doi:10.1177/1010428317710586
32. Che B, Zhang W, Li W, et al. Bacterial lipopolysaccharide-related genes are involved in the invasion and recurrence of prostate cancer and are related to immune escape based on bioinformatics analysis. *Front Oncol*. 2023;13:1141191. doi:10.3389/fonc.2023.1141191
33. Cao L, Ba Y, Chen F, et al. Exploration of bacterial lipopolysaccharide-related genes signature based on T cells for predicting prognosis in colorectal cancer. *Aging*. 2024;16(15):11606–11625. doi:10.18632/aging.206041
34. Bao N, Zhang X, Lin C, et al. A scoring model based on bacterial lipopolysaccharide-related genes to predict prognosis in NSCLC. *Front Genet*. 2024;15:1408000. doi:10.3389/fgene.2024.1408000
35. Walboomers JM, Jacobs MV, Manos MM, et al. Human papillomavirus is a necessary cause of invasive cervical cancer worldwide. *J Pathol*. 1999;189(1):12–19. doi:10.1002/(SICI)1096-9896(199909)189:1<12::AID-PATH431>3.0.CO;2-F
36. Yu L, Wang L, Li M, et al. Expression of toll-like receptor 4 is down-regulated during progression of cervical neoplasia. *Cancer Immunol Immunother*. 2010;59(7):1021–1028. doi:10.1007/s00262-010-0825-1
37. Topalian SL, Drake CG, Pardoll DM. Immune checkpoint blockade: a common denominator approach to cancer therapy. *Cancer Cell*. 2015;27(4):450–461. doi:10.1016/j.ccell.2015.03.001
38. Topalian SL, Taube JM, Pardoll DM. Neoadjuvant checkpoint blockade for cancer immunotherapy. *Science*. 2020;367(6477). doi:10.1126/science.aax0182
39. Livak KJ, Schmittgen TD. Analysis of relative gene expression data using real-time quantitative PCR and the 2(-delta delta C(T)) method. *Methods*. 2001;25(4):402–408.
40. Bannerman DD, Sathyamoorthy M, Goldblum SE. Bacterial lipopolysaccharide disrupts endothelial monolayer integrity and survival signaling events through caspase cleavage of adherens junction proteins. *J Biol Chem*. 1998;273(52):35371–35380. doi:10.1074/jbc.273.52.35371
41. Sica A, Saccani A, Borsatti A, et al. Bacterial lipopolysaccharide rapidly inhibits expression of C-C chemokine receptors in human monocytes. *J Exp Med*. 1997;185(5):969–974. doi:10.1084/jem.185.5.969
42. Chvatchko Y, Hoogewerf AJ, Meyer A, et al. A key role for CC chemokine receptor 4 in lipopolysaccharide-induced endotoxic shock. *J Exp Med*. 2000;191(10):1755–1764. doi:10.1084/jem.191.10.1755
43. Kennel KB, Bozlar M, De Valk AF, et al. Cancer-associated fibroblasts in inflammation and antitumor immunity. *Clin Cancer Res*. 2023;29(6):1009–1016. doi:10.1158/1078-0432.CCR-22-1031

44. Corrales L, Matson V, Flood B, et al. Innate immune signaling and regulation in cancer immunotherapy. *Cell Res*. 2017;27(1):96–108. doi:10.1038/cr.2016.149
45. Liu X, Zhu K, Duan X, et al. Extracellular matrix stiffness modulates host-bacteria interactions and antibiotic therapy of bacterial internalization. *Biomaterials*. 2021;277:121098. doi:10.1016/j.biomaterials.2021.121098
46. Tavakolian S, Goudarzi H, Eslami G, et al. Transcriptional regulation of epithelial to mesenchymal transition related genes by lipopolysaccharide in human cervical cancer cell line HeLa. *Asian Pac J Cancer Prev*. 2019;20(8):2455–2461. doi:10.31557/APJCP.2019.20.8.2455
47. Li H, Wu M, Zhao X. Role of chemokine systems in cancer and inflammatory diseases. *MedComm*. 2022;3(2):e147. doi:10.1002/mco2.147
48. McCully ML, Kouzeli A, Moser B. Peripheral tissue chemokines: homeostatic control of immune surveillance T cells. *Trends Immunol*. 2018;39(9):734–747. doi:10.1016/j.it.2018.06.003
49. Wang N, Liu W, Zheng Y, et al. CXCL1 derived from tumor-associated macrophages promotes breast cancer metastasis via activating NF-κB/SOX4 signaling. *Cell Death Dis*. 2018;9(9):880. doi:10.1038/s41419-018-0876-3
50. Ji HZ, Liu B, Ren M, et al. The CXCLs-CXCR2 axis modulates the cross-communication between tumor-associated neutrophils and tumor cells in cervical cancer. *Expert Rev Clin Immunol*. 2024;20(5):559–569. doi:10.1080/1744666X.2024.2305808
51. Fernandez-Avila L, Castro-Amaya AM, Molina-Pineda A, et al. The value of CXCL1, CXCL2, CXCL3, and CXCL8 as potential prognosis markers in cervical cancer: evidence of E6/E7 from HPV16 and 18 in chemokines regulation. *Biomedicines*. 2023;11(10):2655. doi:10.3390/biomedicines11102655
52. Bhatia R, Kavanagh K, Stewart J, et al. Host chemokine signature as a biomarker for the detection of pre-cancerous cervical lesions. *Oncotarget*. 2018;9(26):18548–18558. doi:10.18632/oncotarget.24946
53. Miyake M, Furuya H, Onishi S, et al. Monoclonal antibody against CXCL1 (HL2401) as a novel agent in suppressing IL6 expression and tumoral growth. *Theranostics*. 2019;9(3):853–867. doi:10.7150/thno.29553
54. Man X, Yang X, Wei Z, et al. High expression level of CXCL1/GROα is linked to advanced stage and worse survival in uterine cervical cancer and facilitates tumor cell malignant processes. *BMC Cancer*. 2022;22(1):712. doi:10.1186/s12885-022-09749-0
55. Zhi W, Ferris D, Sharma A, et al. Twelve serum proteins progressively increase with disease stage in squamous cell cervical cancer patients. *Int J Gynecol Cancer*. 2014;24(6):1085–1092. doi:10.1097/IGC.0000000000000153
56. Kavandi L, Collier MA, Nguyen H, et al. Progesterone and calcitriol attenuate inflammatory cytokines CXCL1 and CXCL2 in ovarian and endometrial cancer cells. *J Cell Biochem*. 2012;113(10):3143–3152. doi:10.1002/jcb.24191
57. Zhang W, Wu Q, Wang C, et al. AKIP1 promotes angiogenesis and tumor growth by upregulating CXC-chemokines in cervical cancer cells. *Mol Cell Biochem*. 2018;448(1–2):311–320. doi:10.1007/s11010-018-3335-7
58. Neefjes J, Jongsma ML, Paul P, et al. Towards a systems understanding of MHC class I and MHC class II antigen presentation. *Nat Rev Immunol*. 2011;11(12):823–836. doi:10.1038/nri3084
59. Axelrod ML, Cook RS, Johnson DB, et al. Biological consequences of MHC-II expression by tumor cells in cancer. *Clin Cancer Res*. 2019;25(8):2392–2402. doi:10.1158/1078-0432.CCR-18-3200
60. Chamuleau ME, Ossenkoppele GJ, van de Loosdrecht AA. MHC class II molecules in tumour immunology: prognostic marker and target for immune modulation. *Immunobiology*. 2006;211(6–8):619–625. doi:10.1016/j.imbio.2006.05.005
61. Mei J, Jiang G, Chen Y, et al. HLA class II molecule HLA-DRA identifies immuno-hot tumors and predicts the therapeutic response to anti-PD-1 immunotherapy in NSCLC. *BMC Cancer*. 2022;22(1):738. doi:10.1186/s12885-022-09840-6
62. Muraoka D, Seo N, Hayashi T, et al. Antigen delivery targeted to tumor-associated macrophages overcomes tumor immune resistance. *J Clin Investig*. 2019;129(3):1278–1294. doi:10.1172/JCI97642
63. Chen Y, Song Y, Du W, et al. Tumor-associated macrophages: an accomplice in solid tumor progression. *J Biomed Sci*. 2019;26(1):78. doi:10.1186/s12929-019-0568-z
64. Tovar Perez JE, Zhang S, Hodgeman W, et al. Epigenetic regulation of major histocompatibility complexes in gastrointestinal malignancies and the potential for clinical interception. *Clin Epigenetics*. 2024;16(1):83. doi:10.1186/s13148-024-01698-8
65. Balakrishnan CK, Tye GJ, Balasubramaniam SD, et al. CD74 and HLA-DRA in cervical carcinogenesis: potential targets for antitumour therapy. *Medicina*. 2022;58(2):190. doi:10.3390/medicina58020190
66. Chen C, Guo Q, Liu Y, et al. Single-cell and spatial transcriptomics reveal POSTN(+) cancer-associated fibroblasts correlated with immune suppression and tumour progression in non-small cell lung cancer. *Clin Transl Med*. 2023;13(12):e1515. doi:10.1002/ctm2.1515
67. Lin SC, Liao YC, Chen PM, et al. Periostin promotes ovarian cancer metastasis by enhancing M2 macrophages and cancer-associated fibroblasts via integrin-mediated NF-κB and TGF-β2 signaling. *J Biomed Sci*. 2022;29(1):109. doi:10.1186/s12929-022-00888-x
68. Karlan BY, Dering J, Walsh C, et al. POSTN/TGFBI-associated stromal signature predicts poor prognosis in serous epithelial ovarian cancer. *Gynecol Oncol*. 2014;132(2):334–342. doi:10.1016/j.ygyno.2013.12.021
69. Huang CQ, Xiao WT, Yao XR, et al. Elevated POSTN expression predicts poor prognosis and is associated with radioresistance in cervical cancer patients treated with radical radiotherapy. *Sci Rep*. 2025;15(1):4174. doi:10.1038/s41598-025-88908-2
70. Sun D, Lu J, Tian H, et al. The impact of POSTN on tumor cell behavior and the tumor microenvironment in lung adenocarcinoma. *Int Immunopharmacol*. 2025;145:113713. doi:10.1016/j.intimp.2024.113713
71. Nielsen NS, Poulsen ET, Lukassen MV, et al. Biochemical mechanisms of aggregation in TGFBI-linked corneal dystrophies. *Prog Retin Eye Res*. 2020;77:100843. doi:10.1016/j.preteyeres.2020.100843
72. Peng D, Fu M, Wang M, et al. Targeting TGF-β signal transduction for fibrosis and cancer therapy. *Mol Cancer*. 2022;21(1):104. doi:10.1186/s12943-022-01569-x
73. Huang H, Tang Q, Li S, et al. TGFBI: a novel therapeutic target for cancer. *Int Immunopharmacol*. 2024;134:112180. doi:10.1016/j.intimp.2024.112180
74. Tian P, Feng Y, Tao L. LINC00460 knockdown sensitizes cervical cancer to cisplatin by downregulating TGFBI. *Chem Biol Drug Des*. 2024;103(1):e14424. doi:10.1111/cbdd.14424
75. Reina-Campos M, Scharping NE, Goldrath AW. CD8(+) T cell metabolism in infection and cancer. *Nat Rev Immunol*. 2021;21(11):718–738. doi:10.1038/s41577-021-00537-8
76. Voskoboinik I, Whisstock JC, Trapani JA. Perforin and granzymes: function, dysfunction and human pathology. *Nat Rev Immunol*. 2015;15(6):388–400. doi:10.1038/nri3839

77. Paul MS, Ohashi PS. The roles of CD8(+) T cell subsets in antitumor immunity. *Trends Cell Biol*. 2020;30(9):695–704. doi:10.1016/j.tcb.2020.06.003
78. Kurachi M. CD8(+) T cell exhaustion. *Semin Immunopathol*. 2019;41(3):327–337. doi:10.1007/s00281-019-00744-5
79. Shapouri-Moghaddam A, Mohammadian S, Vazini H, et al. Macrophage plasticity, polarization, and function in health and disease. *J Cell Physiol*. 2018;233(9):6425–6440. doi:10.1002/jcp.26429
80. Paul S, Chhatar S, Mishra A, et al. Natural killer T cell activation increases iNOS(+)CD206(-) M1 macrophage and controls the growth of solid tumor. *J Immunother Cancer*. 2019;7(1):208. doi:10.1186/s40425-019-0697-7
81. Kruse B, Buzzai AC, Shridhar N, et al. CD4+ T cell-induced inflammatory cell death controls immune-evasive tumours. *Nature*. 2023;618(7967):1033–1040. doi:10.1038/s41586-023-06199-x
82. DeNardo DG, Ruffell B. Macrophages as regulators of tumour immunity and immunotherapy. *Nat Rev Immunol*. 2019;19(6):369–382. doi:10.1038/s41577-019-0127-6
83. Charoentong P, Finotello F, Angelova M, et al. Pan-cancer immunogenomic analyses reveal genotype-immunophenotype relationships and predictors of response to checkpoint blockade. *Cell Rep*. 2017;18(1):248–262. doi:10.1016/j.celrep.2016.12.019
84. Topalian SL, Taube JM, Anders RA, et al. Mechanism-driven biomarkers to guide immune checkpoint blockade in cancer therapy. *Nat Rev Cancer*. 2016;16(5):275–287.
85. Chan TA, Yarchoan M, Jaffee E, et al. Development of tumor mutation burden as an immunotherapy biomarker: utility for the oncology clinic. *Ann Oncol*. 2019;30(1):44–56. doi:10.1093/annonc/mdy495
86. Samstein RM, Lee CH, Shoushtari AN, et al. Tumor mutational load predicts survival after immunotherapy across multiple cancer types. *Nature Genet*. 2019;51(2):202–206. doi:10.1038/s41588-018-0312-8
87. Oh JH, Jang SJ, Kim J, et al. Spontaneous mutations in the single TTN gene represent high tumor mutation burden. *NPJ Genomic Med*. 2020;5:33. doi:10.1038/s41525-019-0107-6
88. Jia Q, Wang J, He N, et al. Titin mutation associated with responsiveness to checkpoint blockades in solid tumors. *JCI Insight*. 2019;4(10). doi:10.1172/jci.insight.127901.
89. Rahangdale L, Lippmann QK, Garcia K, et al. Topical 5-fluorouracil for treatment of cervical intraepithelial neoplasia 2: a randomized controlled trial. *Am J Obstet Gynecol*. 2014;210(4):314.e1–314.e8. doi:10.1016/j.ajog.2013.12.042
90. Denehy TR, Eastman R, SanFilippo L, et al. Bolus mitomycin C and 5-FU with sequential radiation for poor-prognosis locally advanced cervical cancer. *Gynecol Oncol*. 1996;60(1):64–71. doi:10.1006/gyno.1996.0013
91. Bradner WT. Mitomycin C: a clinical update. *Cancer Treat Rev*. 2001;27(1):35–50. doi:10.1053/ctrv.2000.0202
92. Song Y, Wang S. Melatonin synergistically enhances docetaxel induced endoplasmic reticulum stress to promote apoptosis by suppressing NF-κB activation in cervical cancer. *Med Oncol*. 2023;40(8):219. doi:10.1007/s12032-023-02087-6
93. Gupta R, Kadhim MM, Jalil AT, et al. The interactions of docetaxel with tumor microenvironment. *Int Immunopharmacol*. 2023;119:110214. doi:10.1016/j.intimp.2023.110214
94. Alshatwi AA, Periasamy VS, Athinarayanan J, et al. Synergistic anticancer activity of dietary tea polyphenols and bleomycin hydrochloride in human cervical cancer cell: caspase-dependent and independent apoptotic pathways. *Chem Biol Interact*. 2016;247:1–10. doi:10.1016/j.cbi.2016.01.012
95. Krebs HB, Girtanner RE, Nordqvist SR, et al. Treatment of advanced cervical cancer by combination of bleomycin and mitomycin-C. *Cancer*. 1980;46(10):2159–2161. doi:10.1002/1097-0142(19801115)46:10<2159::AID-CNCR2820461009>3.0.CO;2-M
96. Kryczka J, Papiewska-Pajak I, Kowalska MA, et al. Cathepsin B is upregulated and mediates ECM degradation in colon adenocarcinoma HT29 cells overexpressing snail. *Cells*. 2019;8(3).
97. Lee JE, Chung Y, Rhee S, et al. Untold story of human cervical cancers: HPV-negative cervical cancer. *BMB Rep*. 2022;55(9):429–438. doi:10.5483/BMBRep.2022.55.9.042
98. Shi Z, Li H, Song W, et al. Emerging roles of the gut microbiota in cancer immunotherapy. *Front Immunol*. 2023;14:1139821. doi:10.3389/fimmu.2023.1139821

International Journal of Women's Health

Dovepress
Taylor & Francis Group

Publish your work in this journal

The International Journal of Women's Health is an international, peer-reviewed open-access journal publishing original research, reports, editorials, reviews and commentaries on all aspects of women's healthcare including gynecology, obstetrics, and breast cancer. The manuscript management system is completely online and includes a very quick and fair peer-review system, which is all easy to use. Visit http://www.dovepress.com/testimonials.php to read real quotes from published authors.

Submit your manuscript here: https://www.dovepress.com/international-journal-of-womens-health-journal